

# Numerical Analysis for the Oxidation of Phenol with $\text{TiO}_2$ in Wastewater Photocatalytic Reactors

Hisham A. Maddah

Department of Chemical Engineering  
King Abdulaziz University  
Rabigh, Saudi Arabia  
hmaddah@kau.edu.sa

**Abstract**—Phenolic compounds in wastewater (even at low levels) are found to be quite toxic to humans due to their carcinogenic effects. Photocatalysis has been widely studied for the removal of phenol from industrial wastewater. In this study, photocatalytic oxidation of phenol, under UV irradiation in the presence of  $\text{TiO}_2$ , has been numerically investigated. Phenol mass balance and forward finite difference method (explicit) along with various assumed/calculated parameters, from previous works, were used to numerically plot phenol concentration profiles in water with different initial phenol concentrations. Phenol compounds were observed to be totally oxidized at the bottom of the reactor and the maximum conversion rates occur near the reactor walls. It was found that higher irradiation times increase phenol oxidation rates due to higher water hydrolysis. Oxidation rate of phenol (consumption) increases with the increase in initial phenol concentration.

**Keywords**—numerical; water treatment; photochemical; phenol

## I. INTRODUCTION

Photocatalytic reactor is a reactor in which a chemical reaction can take place when there is enough light and catalyst. Photocatalysis term is composed of two words, photo and catalysis. Catalysis refers to the developments in chemical reaction rates for the transformation of reactants into products by the addition of an inert substance that does not get consumed and does not alter the desired product. Catalyst substances increase reaction rates by reducing the required activation energy for that reaction. Particularly, photocatalysis gets the benefits of light and utilizes its energy, using light irradiation, to activate the added catalyst substances that modify the chemical reaction rate without being involved and/or consumed [1, 2]. Chlorophyll of plants is a typical natural photocatalyst (vital for photosynthesis). The difference between chlorophyll and synthesized titanium dioxide ( $\text{TiO}_2$ ) photocatalysts [4], is that chlorophyll molecules absorb energy from sunlight to turn water and carbon dioxide into oxygen and glucose, whereas  $\text{TiO}_2$  creates strong oxidation agents and electronic holes to breakdown the organic matter to carbon dioxide and water when light is available [3, 4].

The worldwide demand on fresh/clean water has been increasing enormously [5-7] due to the fact that water has always been prioritized as a top necessity for human beings [8].

Sources of freshwater including rivers, lakes, snow packs, wetlands and aquifers make up a very small fraction (only 2.5 percent) of all water on the planet [9]. Thus, improving current water treatment technologies is necessary to meet the growing demand on drinking water. Wastewater such as industrial wastewater contains heavy metals, toxic organics (e.g. phenol compounds) and other dissolved solids that may pose serious health risks on humans [10]. Photocatalysis has been widely studied for the removal of organic contaminants (e.g. phenol) from industrial wastewater. Numerous studies showed that  $\text{TiO}_2$  has received considerable attention as a promising catalyst since it has been used for optical coatings, photocatalysis agents, electrodes, gas sensors, solar cells and hydrogen storage [1, 11, 12]. The objective of this study is to analyze and investigate the concentration decay of phenol in water during the photocatalytic oxidation process under UV irradiation and in the presence of  $\text{TiO}_2$ . The effect of both initial phenol concentration and irradiation time on phenol decomposition have been numerically determined. Oxidation reaction was assumed to be at steady state and therefore phenol concentration profiles were numerically plotted as a function of reactor height and radius. Several parameters such as initial phenol concentrations,  $\text{TiO}_2$  catalyst weight, reactor height, internal radius, external radius, diffusivity, velocity and phenol oxidation rate have been either assumed, calculated from experiments and/or taken from previous works to carry out our numerical analysis. The novelty of this work is associated with the numerical determination of the decay in phenol concentration profiles in industrial wastewater when using advanced oxidation processes (AOPs) as UV/ $\text{TiO}_2$  with different initial phenol concentrations. Determined phenol profiles would help future studies to build upon the visualized concentration change inside photocatalytic reactors.

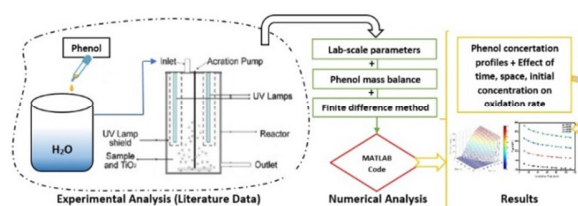


Fig. 1. Framework

## II. PHOTOCATALYSIS MECHANISM

When TiO<sub>2</sub> absorbs UV radiation from sunlight or an illuminated light source (fluorescent lamps), it will produce pairs of electrons and holes. Electron of the valence band of titanium dioxide becomes excited when illuminated by light. Excess energy of this excited electron promotes the electron to a conduction band creating a negative-electron ( $e^-$ ) and a positive-hole ( $h^+$ ) pair. This stage is referred to as the semiconductor's photo-excitation state. The energy difference between the valence band and the conduction band is known as the band gap. Wavelength of light necessary for photo-excitation is 388nm that is calculated from dividing 1240 by band gap energy (3.2eV) where  $E(\text{eV})=120/\lambda$  (nm). In Figure 2, the positive-hole of titanium dioxide breaks water molecules apart to form hydrogen gas and a hydroxyl radical [1]. The negative-electron reacts with an oxygen molecule to form a super oxide anion. This cycle continues when light is available [13].

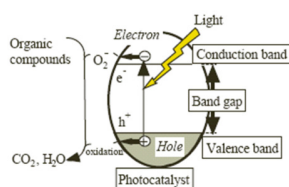
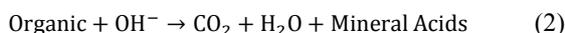


Fig. 2. Photocatalysis mechanism

Photocatalytic destruction of organic compounds depends on understanding semiconductor photochemistry. Photocatalytic oxidation often proceeds via adsorption of organic pollutants on the catalyst surface, followed by a direct subtraction of the pollutant's electrons by positively charged holes. Another possible way is oxidation with OH radicals generated from an aqueous environment that takes place at the catalyst surface and its vicinity. Both reactions may proceed simultaneously and the dominance preference depends on both chemical and adsorption properties of the pollutant. Normally, two simple reactions, as shown in (1) and (2), occur to generate hydroxyl radicals that will be reacted with the organic pollutant and convert it to carbon dioxide and clean water [14, 15].



## III. TITANIUM DIOXIDE CATALYST

Titanium dioxide in photocatalytic reactors is the most common efficient, feasible and inexpensive way to remove phenol. Titanium dioxide is considered cheap, it is insoluble in water, harmless, resistant to most chemicals and highly active to light [1]. Recent studies showed that photocatalytic reactors are promising for the removal of phenol from water by using TiO<sub>2</sub> as a catalyst where phenol and its dihydroxy derivatives undergo destruction in the presence of illuminated TiO<sub>2</sub> according to first order kinetics [1, 16-18]. Titanium dioxide exists in different crystalline forms, anatase, rutile and brookite, with its bandgap around 3.2eV and is activated only under ultraviolet (UV) light (about 8% of solar energy) [19-23]. TiO<sub>2</sub> is a semiconductor material with large surface energy,

interesting quantum effect and high specific surface area which ensure its applicability in photocatalytic applications including water splitting, organic decomposition and energy harvesting. Also, TiO<sub>2</sub> is preferred over other semiconductors due to its high reactivity, long-term chemical stability, low cost, nontoxicity and corrosion resistivity. TiO<sub>2</sub>/UV irradiation systems enable water splitting and the generation of hydroxyl radicals (oxygen and hydrogen) that will be reacted with undesired organics to produce clean water [12]. Pure TiO<sub>2</sub> is commercially available and can be synthesized in the laboratory. The specific surface area (SSA) of the catalyst mixture depends on the purity of TiO<sub>2</sub>. Pure TiO<sub>2</sub> (Aldrich, >99% anatase) SSA can reach up to 7.1m<sup>2</sup>g<sup>-1</sup>. More details about the physicochemical characterization and quantitative values of the optical properties of TiO<sub>2</sub> catalysts suspensions can be found in [24-26].

## IV. LITERATURE ON MODELING OF REACTION RATES

Modeling of photocatalytic reaction rates can be expressed by a set of ordinary differential equations (3), where each equation is established for the key chemical species in the photocatalytic reactor. Equation (3) can be reduced to (4) with the following assumptions: (a) batch mode operation, (b) the weight of irradiation catalyst ( $W_{irr}$ ) is known and (c) mixing is high enough so that reaction rate constant can be defined in the irradiation reactor section. Our assumptions are valid for reactors with suspended or immobilized TiO<sub>2</sub> [14].

$$V \frac{dC_i}{dt} = [\sum v_{i,k} R_k] W_{irr} \quad (3)$$

$$r_1 = \frac{V}{W_{irr}} \frac{dC_i}{dt} = \sum v_{i,k} R_k \quad (4)$$

where  $V$  is the total reactor volume, (L),  $C_i$  is the concentration of the  $i$  chemical species ( $\text{g}\cdot\text{L}^{-1}$ ),  $t$  is the reaction time (s),  $v_{i,k}$  is a dimensionless stoichiometric coefficient for  $i$  species involved in reaction step  $k$ ,  $R_k$  is the photoconversion rate of step  $k$ ,  $W_{irr}$  is the unit weight of irradiation catalyst ( $\text{mol}\cdot\text{g}_{cat}^{-1}$ ).

Most of the previous contributions devoted to the photocatalytic oxidation of phenol are focused on how the reaction rate is influenced by different catalyst loading, phenol concentration, pH, presence of inorganic species and additional oxidants such as ozone or hydrogen peroxide [27-30]. Developments have been reported at a pilot plant scale for the photocatalytic treatment of phenol in effluents derived from integrated gasification combined cycle (IGCC) power plants [31] and electroplating factories [32], including their economic assessment, but without considering engineering models to verify the scaling-up predictions from laboratory data. A few kinetic studies concluded that dependence of the reaction rate of phenol follows the Langmuir-Hinshelwood kinetic equation [28-30]. However, Langmuir-Hinshelwood kinetic equations do not consider explicitly the local radiation absorption rate inside the photoreactor leading to equations that are only valid for the experimental setup with estimated parameters (assumptions), making those models invalid for the design of photoreactors. It is necessary to determine intrinsic kinetic models that will allow us to describe the influence of the local volumetric rate of photon absorption (LVRPA) on the reaction rate in any position of the photoreactor volume [33-36].

Development of supported catalysts in form of fixed beds, fluidized beds or slurries is vital to avoid catalyst recovery costs and other concerns about a potential toxicity of titanium dioxide nanoparticles [37, 38].

## V. PHOTOCATALYTIC REACTORS

Laboratory scale and bench scale photoreactors were previously designed and studied for the removal of numerous pollutants (e.g. phenol and/or cyanide) from wastewater by catalytic oxidation under UV irradiation. Required components and design setup of a laboratory/bench scale photoreactor used for wastewater treatment can be seen in [31]. Typically, lab scale photoreactors are designed in a cylindrical shape with a total volume of 120cm<sup>3</sup> operating in a closed recirculating circuit driven by a centrifugal pump and with a stirred reservoir tank equipped with a device for withdrawal of samples. Illumination can be carried out by an Osram Ultramed 400W UV metal halide lamp that provides a high UVA irradiation with a controlled radiation flux values using neutral filters. It is possible to validate the scaling-up methodology with the bench scale photoreactor setup that has a total irradiation volume of 1250cm<sup>3</sup> (ten times higher than the laboratory scale). More details regarding the discussed reactor design (which was studied for cyanide removal and not phenol) such as dimensions, lamp type/position, electrical input power, UV emission spectrum and radiation flux can be found in [24-26]. A scaling-up methodology for the photocatalytic oxidation of phenol was studied and proposed in [31, 39]. Scaling-up methodology depends on the experimental determination of the intrinsic kinetic parameters at a laboratory scale, in order to predict the performance of larger scale reactors without any adjustable parameters. This method was found to be valid in a bench scale photoreactor with different geometries and irradiation sources, both with commercial TiO<sub>2</sub> and silica-supported TiO<sub>2</sub>. Designing of a large photocatalytic reactor requires the determination of species mass balances to predict the macroscopic conversion of reactants [31, 39]. The kinetic model expresses the evaluation of the reaction rate with parameters based on phenomenological basis. Simple equations of the Langmuir-Hinshelwood kinetic model only take into account the concentration of reactants and products, whereas the effect of the catalyst concentration and the radiation flux are considered implicitly in the kinetic constants. Thus, the derived kinetic expressions are only valid for the developed experimental setup and cannot be extrapolated to other reactor configurations. Kinetic models must be independent of the experimental features of the reactor and must be determined based on the detailed reaction mechanism of the process, including the radiation steps and therefore the rate of photon absorption. Prior to the resolution of the mass balances calculations, the radiation field in the irradiated volume of the photoreactor must be modeled and evaluated. The inevitable radiation profiles that present in photocatalytic reactors lead to non-uniform distributions of the local values of the radiation absorption rates and thus of the reaction rates [31, 39].

The validation of the proposed kinetic scheme and the parameters' values are recognized by an optimization algorithm that minimizes the error between the experimental results and the predicted values. Once the intrinsic kinetics of the process

are obtained exclusively from laboratory data, the design of the large-scale photoreactor becomes easy to determine. Obviously, the construction of the designed photoreactor as well as the comparison of its experimental conversions with the simulated values would validate the whole scaling-up procedure.

## VI. METHODOLOGY AND MODELING EQUATIONS

Intrinsic kinetics in the laboratory scale photoreactor (with similar reactor dimensions and data from previous studies) were utilized to numerically obtain photocatalytic phenol oxidation rate, phenol mass balance in the reservoir tank and phenol concentration profiles at a specific TiO<sub>2</sub> catalyst weight, assuming that: (a) the system is perfectly mixed, (b) there are no mass transport limitations, (c) the conversion per pass in the reactor is differential, and (d) there are no parallel dark reactions, the mass balance can be expressed as follows:

$$\frac{dC_{ph} t}{dt} |_{Tank} = -\frac{V_{React}}{V_{Tot}} \langle R_{ph}(x, t) \rangle_{V_{React}} \quad (5)$$

where  $C_{ph}$  is the phenol molar concentration,  $V$  is the volume,  $Tank$ ,  $React$  and  $Tot$  subscripts refer to the tank, reactor and total, respectively,  $t$  denotes reaction time,  $x$  denotes reaction position in space and  $R_{ph}(x, t)$  is the phenol oxidation rate as a function of both space (reactor height) and time (reaction time). Average reaction rate (phenol oxidation rate) was calculated from (6) which was derived from discussed kinetic models. Kinetic developments normally depend on the perceived reaction mechanism which explicitly refers to the spatial variations of the LVRPA produced by the inevitable radiation profiles existing in the photoreactor [33].

$$R_{ph} = -S_g C_{cat} \frac{\alpha_1 C_{ph}}{1 + \alpha_3 C_{ph}} \left[ -1 + \sqrt{1 + \frac{\alpha_2}{S_g C_{cat}} e^a} \right] \quad (6)$$

where  $R_{ph}$  is the phenol disappearance rate,  $S_g$  is the catalyst specific surface area,  $C_{cat}$  is the catalyst mass concentration,  $C_{ph}$  is the phenol molar concentration,  $e^a$  is the LVRPA, and  $\alpha_i$  ( $i=1$  to 3) are the kinetic parameters. Selected phenol molar concentrations (initial) were 200, 300, 400 and 500mg/L.

According to (6), the evaluation of the reaction rate requires the estimation of the radiation field inside the photoreactor in order to calculate the LVRPA. Authors in [31] estimated the LVRPA ( $e^a$ ) value of  $8.93 \times 10^{-9} \text{ Einstein cm}^{-3} \text{ s}^{-1}$  in the laboratory scale photoreactor for cyanide oxidation with TiO<sub>2</sub> (which was assumed to be similar for phenol oxidation with TiO<sub>2</sub>). TiO<sub>2</sub> specific surface area was selected from literature as:  $S_g = 240 \text{ m}^2 \text{ g}^{-1}$ . Kinetic parameters  $\alpha_1$ ,  $\alpha_2$  and  $\alpha_3$  for TiO<sub>2</sub> have been previously estimated from experimental and simulation analysis of cyanide oxidation using a Marquardt-Levenberg non-linear regression algorithm. For simplicity, the values of the obtained kinetic parameters for cyanide oxidation are assumed to be similar for phenol oxidation, which were:

$$\alpha_1 = 6.43 \times 10^{-6} \text{ cm s}^{-1}$$

$$\alpha_2 = 1.64 \times 10^{11} \text{ cm}^2 \text{ s Einstein}^{-1}$$

$$\alpha_3 = 0 \text{ cm}^3 \text{ mol}^{-1}$$

and then phenol disappearance rates were calculated from (6) for the four phenol initial concentrations (200, 300, 400 and 500mg/L) with TiO<sub>2</sub> catalyst weight of 0.5g·cm<sup>-3</sup> as shown in Table I. Oxidation rate of every phenol concentration was determined from taking the same TiO<sub>2</sub> catalyst weight of 0.5g·cm<sup>-3</sup> [28, 29, 31, 33].

TABLE I. DATA FOR DISAPPEARANCE RATE CALCULATIONS\*

Initial phenol concentration $C_{ph}$ (ppm) [g cm <sup>-3</sup> ]	Kinetic parameters
200 [ $2 \times 10^{-4}$ ]	$\alpha_1 = 6.43 \times 10^{-6}$ cm s <sup>-1</sup>
300 [ $3 \times 10^{-4}$ ]	$\alpha_2 = 1.64 \times 10^{11}$ cm <sup>2</sup> s Einstein <sup>-1</sup>
400 [ $4 \times 10^{-4}$ ]	$\alpha_3 = 0$ cm <sup>3</sup> mol <sup>-1</sup>
500 [ $5 \times 10^{-4}$ ]	

\* $S_g = 240$  m<sup>2</sup> g<sup>-1</sup>,  $e^a = 8.93 \times 10^{-9}$  Einstein cm<sup>-3</sup> s<sup>-1</sup>

It is important to remark that the intrinsic kinetic model determined in the laboratory reactor from (5) is applicable when other reactor configurations have light sources with a similar spectral distribution of the emitted radiation. Hence, we can assume that obtained kinetic parameters for (6) are reasonable approximations and they are valid for the bench scale system [25, 33]. Modeling and simulation of phenol concentration profile (oxidation rate) inside the photocatalytic reactor can be computed from the phenol mass balance equation in (7). A differential form of the mass conservation equation was used under the following assumptions: (a) steady state, (b) negligible thermal effects, (c) unidirectional vertical flow with symmetry, (d) negligible diffusion when compared to the convective flux, (e) incompressible flow (constant  $\rho$ ), and (f) constant diffusion coefficient ( $D_{ph-water} = 9.1 \times 10^{-6}$  cm<sup>2</sup>·s<sup>-1</sup>) [40]. Phenol mass balance can be expressed in cylindrical coordinates as [25, 33]:

$$v_z(r) \frac{\partial C_{ph}(z,r)}{\partial z} = D_{ph-Water} \left[ \frac{1}{r} \frac{\partial}{\partial r} \left( r \frac{\partial C_{ph}(z,r)}{\partial r} \right) \right] + R_{ph}(z,r) \quad (7)$$

where  $z$  and  $r$  refer to reactor height and radii difference between inlet/outlet cylinders, respectively. The boundary conditions for solving (7) are derived from the following assumptions: (a) the nominal reactor height,  $H$ , coincides with the effective height and (b) the reactor walls are non-permeable [25, 33]:

$$C_{ph}(H,r) = C_0 \quad (8)$$

$$\frac{\partial C_{ph}(z,r_{int})}{\partial r} = \frac{\partial C_{ph}(z,r_{ext})}{\partial r} = 0 \quad (9)$$

The resolution of (7) requires the estimation of the velocity profile in the annular space,  $v_z(r)$ , that was calculated from (10) and under the assumptions: (a) laminar flow regime, (b) Newtonian fluid, and (c) negligible end effects. Assuming internal and external radii are 5cm and 7cm respectively,  $\chi = r_{int}/r_{ext}$ ,  $\langle v_z \rangle$  is 6ml/min<sup>-1</sup> representing the average velocity, and the velocity is constant under incompressible flow conditions and must be a positive value [25, 33].

$$v_z(r) = 2 \langle v_z \rangle \left\{ \frac{1 - (r/r_{ext})^2 + \left[ \frac{1 - \chi^2}{\ln(1/\chi)} \right] \ln(r/r_{ext})}{\frac{1 - \chi^4}{1 - \chi^2} - \frac{1 - \chi^2}{\ln(1/\chi)}} \right\} \quad (10)$$

The solution of the phenol differential mass balance in the photoreactor in (7) requires the description of the reaction rate  $R_{ph}(z,r)$  given by the intrinsic kinetic model determined at

the laboratory scale from (6) assuming that  $R_{ph}(z,r) = R_{ph} = \text{constant}$ . We may simplify the mass balance equation (7) to (11) – (15) with the assumptions:  $v_z(r) = \text{constant} = v_z(\bar{r})$ ;  $\bar{r} = (r_{in} + r_{ext})/2$  and  $R_{ph}(z,r) = \text{constant} = R_{ph}$ :

$$\frac{\partial C_{ph}(z,r)}{\partial z} = \frac{D_{ph-Water}}{v_z} \left[ \frac{1}{r} \frac{\partial}{\partial r} \left( r \frac{\partial C_{ph}(z,r)}{\partial r} \right) \right] + \frac{R_{ph}}{v_z} \quad (11)$$

$$\frac{\partial C_{ph}(z,r)}{\partial z} = \beta \left[ \frac{1}{r} \frac{\partial}{\partial r} \left( r \frac{\partial C_{ph}(z,r)}{\partial r} \right) \right] + m \quad (12)$$

$$\beta = \frac{D_{ph-Water}}{v_z} \quad (13)$$

$$m = \frac{R_{ph}}{v_z} \quad (14)$$

Let  $C_{ph}(z,r) = C(z,r) = C$ . Equation (12) becomes (15):

$$\frac{\partial C}{\partial z} = \beta \frac{\partial C}{\partial r} \left[ 1 + r^* \frac{\partial C}{\partial r} \right] + m \quad (15)$$

A forward finite difference method (explicit) with neglecting higher orders [41], or called finite divided difference [42], was used to obtain the phenol concentration profile inside the reactor from the simplified mass balance equation (15), while assuming ( $r^* = \bar{r}$ ) to give the following:

$$\frac{C_i^{n+1} - C_i^n}{\Delta z} = \beta \frac{C_{i+1}^n - C_i^n}{\Delta r} \left[ 1 + \bar{r} \frac{C_{i+1}^n - C_i^n}{\Delta r} \right] + m \quad (16)$$

$$C_i^{n+1} = \beta \Delta z \left( \frac{C_{i+1}^n - C_i^n}{\Delta r} \right) \left[ 1 + \bar{r} \frac{C_{i+1}^n - C_i^n}{\Delta r} \right] + m \Delta z + C_i^n \quad (17)$$

$$C_i^{n+1} = \beta \Delta z \left( \frac{C_{i+1}^n - C_i^n}{\Delta r} \right) \left[ 1 + \frac{(r_{in} + r_{ext})(C_{i+1}^n - C_i^n)}{2\Delta r} \right] \dots \dots \dots + m \Delta z + C_i^n \quad (18)$$

Phenol concentration profile was numerically identified from (18) by using MATLAB, where  $(i,n) = (z,r)$  is referring to change steps in concentration (in two {for} loops) of reactor height and radius, with the known and/or calculated data of the total reactor system including reactor geometry, reactant (phenol in water) and catalyst (TiO<sub>2</sub>) concentration. Table II shows the reactor system parameters and their selected/calculated values that were plugged into MATLAB for further analysis.

## VII. RESULTS AND DISCUSSION

Since modeling and simulation analysis was carried out for understanding and visualizing phenol degradation rate inside the reactor, phenol concentration profile and the effect of irradiation time and initial phenol concentration on the oxidation rate of phenol have been investigated.

### A. Phenol Concentration Profile inside the Photoreactor

Phenol concentration profiles of wastewater with various initial phenol concentrations of 200, 300, 400 and 500mg/L are plotted in Figures 3-6. Understanding the plotted concentration profiles will help us to achieve better phenol degradation rate. It was observed that phenol compounds get totally oxidized at the bottom of the reactor (when wastewater is fed from reactor top-side) and that the maximum conversion rates (i.e. phenol concentration is zero) occur near the reactor walls ( $r=5$ cm and/or  $r=7$ cm, since there should identical figures from the symmetry boundary conditions), while lower phenol

conversion rates occur at the center of the reactor ( $r=6\text{cm}$ ). Lower velocities adjacent to the walls increases the contact time between the catalyst and phenol, hence, higher irradiation time is maintained, thus, higher conversion is observed. Most of the phenol gets consumed at the top-side of the reactor (near the inlet) when initial phenol concentration is less than  $200\text{mg/L}$ . However, increase in initial phenol concentration leads to higher phenol diffusion along reactor height which indicates that higher oxidation times are required for the complete oxidation of high initial concentrations of phenol in water.

TABLE II. PHOTO-CATALYTIC REACTOR PARAMETERS

Parameter	Symbol (unit)	Value/Comments
Initial phenol concentration	$C_i$ (ppm)	200, 300, 400, 500
Catalyst weight ( $\text{TiO}_2$ )	$C_{cat}$ ( $\text{g cm}^{-3}$ )	0.5
Reactor height	$H$ (cm)	35
Reactor internal radius	$r_{in}$ (cm)	5
Reactor external radius	$r_{ext}$ (cm)	7
Phenol-water diffusivity	$D_{ph-water}$ ( $\text{cm}^2 \text{s}^{-1}$ )	$9.10 \times 10^{-6}$
Velocity*	$v_z$ ( $\text{mL s}^{-1}$ )	25
Reactor volume**	$V_{React}$ ( $\text{cm}^3$ )	2639
Total volume**	$V_{tot}$ ( $\text{cm}^3$ )	7917
Reactor/total volume ratio	$V_{React}/V_{tot}$ (N/A)	0.33
Phenol oxidation rate***	$R_{ph}$ ( $\text{mol cm}^{-3} \text{s}^{-1}$ )	$(3.3, 5, 6.6 \text{ and } 8.3) \times (-10^{-7})$ for 200, 300, 400 and 500 mg/L, respectively.
Defined constant, (13)	$\beta$ ( $\text{cm}^2 \text{mL}^{-1}$ )	$3.64 \times 10^{-7}$
Defined constant, (14)	$m$ ( $\text{mol mL}^{-2}$ )	$(1.23, 2, 2.64, 3.32) \times (-10^{-8})$ for 200, 300, 400 and 500 mg/L, respectively.

\*Calculated at  $r = 6 \text{ cm}$ ; that is the averaged value between  $r_{in}$  and  $r_{ext}$

\*\*Reactor and total system volumes were calculated from  $V = \pi r^2 h$  at  $r_{in}$  and  $r_{ext}$  for inner and outer cylinders as ( $V_{in}$ ) and ( $V_{out} = V_{tot}$ ), respectively, where  $V_{React} = V_{out} - V_{in}$  and total volume was assumed to be  $V_{tot} = 3V_{React}$

\*\*\*Oxidation rate of every phenol concentration (mg/L) was calculated directly from using the averaged catalyst weight  $0.5 \text{ g cm}^{-3}$  in (6).

B. Effect of Irradiation Time on Phenol Oxidation Rate

Higher irradiation times increase phenol oxidation rates within the reactor as shown in Figure 4 due to the following reasons: (a) probability of occurrence of water hydrolysis increases with higher irradiation times, (b) number of produced free hydroxyl groups (OH) in water should be increased with more water hydrolysis, (c) phenolic compounds get reacted (consumed) with free hydroxyl groups, as explained previously in (2), to produce clean water with mineral acids and release carbon dioxide to the atmosphere.

C. Effect of Initial Concentration on Phenol Oxidation Rate

Production rates of phenol ( $R_{ph}$ ) were determined for the four studied initial phenol concentrations 200, 300, 400 and  $500\text{mg/L}$  as shown in Figure 5. Rates were calculated from using the assumed catalyst weight of  $0.5\text{g}\cdot\text{cm}^{-3}$  at every selected initial concentration. Obviously, production rates of phenol were found to be in negative values which indicate that phenol is oxidized and consumed from water during the photocatalytic reaction. Oxidation rate of phenol increases with the increase in initial phenol concentration as concluded from

obtained production rates of  $-3.3 \times 10^{-7}$  and  $-8.2 \times 10^{-7} \text{ mol}\cdot\text{cm}^{-3}\cdot\text{s}^{-1}$  for 200 and  $500\text{mg/L}$ , respectively.

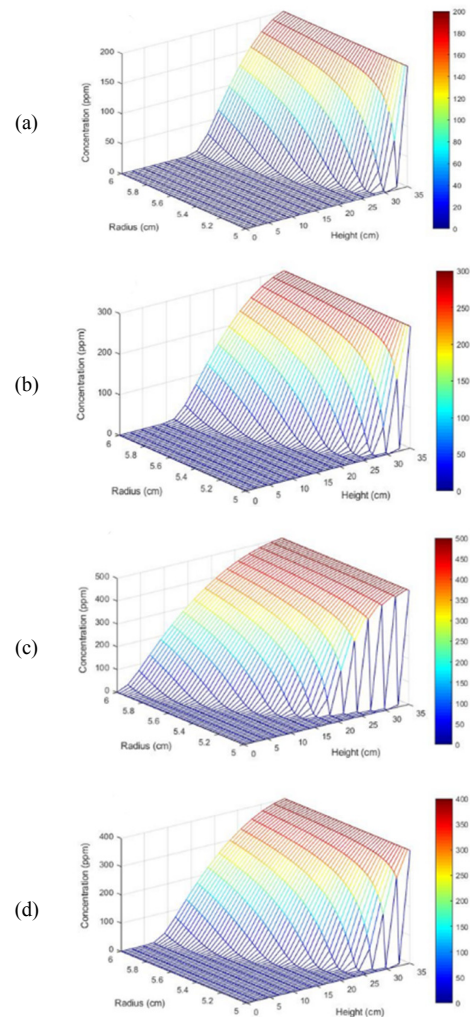


Fig. 3. Phenol concentration profile as a function of reactor height and reactor half-radius.  $\text{TiO}_2$  concentration:  $0.5\text{g}\cdot\text{cm}^{-3}$  and inlet phenol concentrations: (a)  $200\text{mg/L}$ , (b)  $300\text{mg/L}$ , (c)  $400\text{mg/L}$ , (d)  $500\text{mg/L}$ , calculated from (7) and (18). Note that [ppm]=[mg/L].

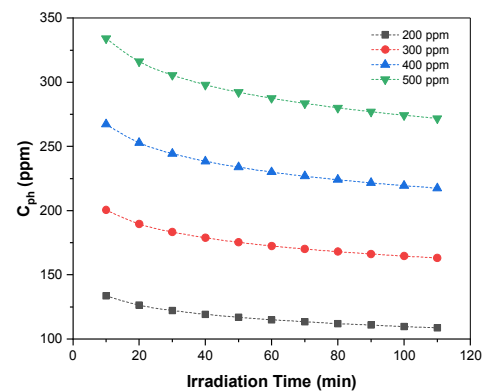


Fig. 4. Effect of irradiation time on phenol oxidation rate at different inlet phenol concentrations. Note that [ppm]=[mg/L].

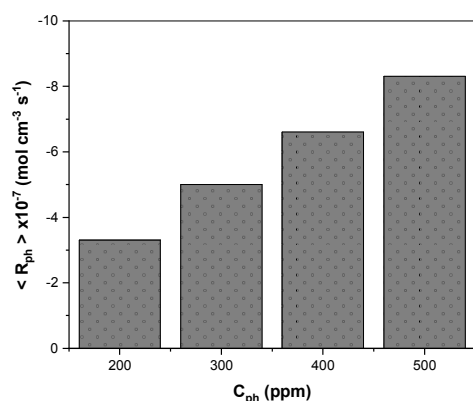


Fig. 5. Effect of initial phenol concentration on phenol oxidation rate at different inlet phenol concentrations. Note that [ppm]=[mg/L].

For comparison purposes, we went through the literature to check our numerical estimated removal efficiency with previous experimental works as shown in Table III. Authors in [43] found that phenol removal efficiency through AOPs (UV/TiO<sub>2</sub>) ranges from 6% to 55% depending on many variables such as TiO<sub>2</sub> wt. %, light intensity, reaction time and pH. In contrast, our findings showed a 45% phenol removal efficiency which is comparable the removal efficiency of 50% found in. Authors in [44] found out that the lower the water pH, the more the phenol removal efficiency we get and that approximately 85% of phenol was removed by using TiO<sub>2</sub> (anatase) at pH 3.5 whereas only 70% removal efficiency was observed at pH 6.5. In a more recent study, 58.8% phenol removal efficiency at pH 8 was observed [45]. It is worth mentioning that our study data were calculated and/or assumed from previous literature (except for the removal efficiency) to estimate the removal efficiency and carry out the numerical analysis.

Obtained results predicted that phenol compounds can be totally oxidized at the bottom of the reactor if there are enough radiation time and appropriate catalyst concentration. Our findings also confirmed that photocatalytic reactors with higher irradiation times increase phenol oxidation rates due to higher water hydrolysis; oxidation rate of phenol (consumption) increases with the increase in initial phenol concentration.

TABLE III. COMPARISON BETWEEN LITERATURE DATA AND DETERMINED EFFICIENCY OF UV/TiO<sub>2</sub>

$C_i$ (mg/L)	$C_{cat}$ (g cm <sup>-3</sup> )	pH	$t$ (h)	$\eta$ (%)	$R_{ph}$ (mol cm <sup>-3</sup> s <sup>-1</sup> )	Ref.
2000	0.0025	6.5	20	50	N/A	[43]
94.11	0.0062	3.5	1	85	$-11.9 \times 10^{-10}$	[44]
94.11	0.0062	6.5	1	70	$-6.8 \times 10^{-10}$	[44]
100	0.1 (w/w%)	8	1	58.8	$-2.65 \times 10^{-10}$	[45]
350	0.5	7	2	45	$-5.8 \times 10^{-7}$	[*]

\*This study. Averaged data of assumed phenol concentration, TiO<sub>2</sub> wt. %, pH, time and oxidation rate were assumed and/or calculated to estimate phenol removal efficiency.  $\eta$  refers to phenol removal efficiency. All other symbols are defined in Table II.

### VIII. CONCLUSIONS

The concentration decay of phenol in water during the photocatalytic oxidation process, under UV irradiation and in the presence of TiO<sub>2</sub>, has been numerically investigated. Phenol mass balance, oxidation rate and velocity equations

along with forward finite difference method (explicit) and assumed/calculated parameters were used to numerically plot phenol concentration profiles, as a function of reactor height and radius, for different initial phenol concentrations mimicking organics in industrial wastewater. It was observed that phenol compounds get totally oxidized at the bottom of the reactor and that maximum conversion rates occur near the reactor walls. When initial phenol concentration is low, most of the phenol gets consumed once it enters the reactor because low phenol concentrations require lower radiation times and catalysts. However, in general, higher irradiation times increase phenol oxidation rates within the reactor due to higher water hydrolysis which produce numerous free hydroxyl groups (OH) to be reacted with phenolic compounds. Also, it was found that oxidation rate of phenol (consumption) increases with the increase in initial phenol concentration.

### REFERENCES

- [1] H. A. Maddah, "Optimal operating conditions in designing photocatalytic reactor for removal of phenol from wastewater", ARPN Journal of Engineering and Applied Sciences, Vol. 11, No. 3, pp. 1799-1802, 2016
- [2] J. M. Herrmann, "Heterogeneous photocatalysis: fundamentals and applications to the removal of various types of aqueous pollutants", Catalysis Today, Vol. 53, No. 1, pp. 115-129, 1999
- [3] D. R. Fruge, G. D. Fong, F. K. Fong, "Photosynthesis of Polyatomic Organic Molecules From Carbon Dioxide and Water by the Photocatalytic Action of Visible-Light-Illuminated Platinized Chlorophyll a Dihydrate Polycrystals", Journal of the American Chemical Society, Vol. 101, No. 13, pp. 3694-3697, 1979
- [4] Green Earth Nano Science, "What is Photocatalyst?", available at: <http://www.mchnanosolutions.com/whatis.html>, 2012
- [5] H. Maddah, A. Chogle, "Biofouling in reverse osmosis: phenomena, monitoring, controlling and remediation", Applied Water Science, Vol. 7, No. 6, pp. 2637-2651, 2016
- [6] H. A. Maddah, A. M. Chogle, "Applicability of low pressure membranes for wastewater treatment with cost study analyses", Membrane Water Treatment, Vol. 6, No. 6, pp. 477-488, 2015
- [7] H. A. Maddah, "Modeling the Feasibility of Employing Solar Energy for Water Distillation", in: Handbook of Environmental Materials Management, pp. 1-25, Springer, 2018
- [8] H. A. Maddah, A. S. Alzhrani, "Quality Monitoring of Various Local and Imported Brands of Bottled Drinking Water in Saudi Arabia", World Journal of Engineering and Technology, Vol. 5, No. 4, pp. 551-563, 2017
- [9] H. A. Maddah, "Modeling the Relation between Carbon Dioxide Emissions and Sea Level Rise for the Determination of Future (2100) Sea Level", American Journal of Environmental Engineering, Vol. 6, No. 2, pp. 52-61, 2016
- [10] H. A. Maddah, A. S. Alzhrani, A. M. Almalki, M. Bassyouni, M. H. Abdel-Aziz, M. Zoromba, M. A. Shihon "Determination of the treatment efficiency of different commercial membrane modules for the treatment of groundwater", Journal of Materials and Environmental Sciences, Vol. 8, No. 6, pp. 2006-2012, 2017
- [11] M. A. Worsley, J. D. Kuntz, P. J. Pauzaskie, O. Cervantes, J. M. Zaugg, A. E. Gash, J. H. Satcher Jr, T. F. Baumann, "High surface area carbon nanotube-supported titanium carbonitride aerogels", Journal of Materials Chemistry, Vol. 19, No. 31, p. 5503, 2009
- [12] S. Stankovich, D. A. Dikin, G. H. B. Dommett, K. M. Kohlhaas, E. Zimney, E. A. Stach, R. D. Piner, S. Nguyen, R. Ruoff, "Graphene-based composite materials", Nature, Vol. 442, No. 7100, pp. 282-286, 2006
- [13] A. G. Agrios, P. Pichat, "State of the art and perspectives on materials and applications of photocatalysis over TiO<sub>2</sub>", Journal of Applied Electrochemistry, Vol. 35, No. 7-8, pp. 655-663, 2005

- [14] H. De Lasa, B. Serrano, M. Salaiques, Photocatalytic Reaction Engineering, Springer Science & Business Media, 2005
- [15] A. Mills, R. H. Davies, D. Worsley, "Water purification by semiconductor photocatalysis", Chemical Society Reviews, Vol. 22, No. 6, pp. 417-425, 1993
- [16] A. Sobczynski, L. Duczmal, W. Zmudzinski, "Phenol destruction by photocatalysis on TiO<sub>2</sub>: An attempt to solve the reaction mechanism", Journal of Molecular Catalysis A: Chemical, Vol. 213, No. 2, pp. 225-230, 2004
- [17] S. P. Devipriya, S. Yesodharan, "Photocatalytic degradation of phenol in water using TiO<sub>2</sub> and ZnO", Journal of Environmental Biology, Vol. 31, No. 3, pp. 247-249, 2010
- [18] R. M. Abhang, D. Kumar, S. V. Taralkar, "Design of Photocatalytic Reactor for Degradation of Phenol in Wastewater", International Journal of Chemical Engineering and Applications, Vol. 2, No. 5, pp. 337-341, 2011
- [19] B. Marinho, M. Ghislandi, E. Tkalya, C. E. Koning, G. de With, "Electrical conductivity of compacts of graphene, multi-wall carbon nanotubes, carbon black, and graphite powder", Powder Technology, Vol. 221, pp. 351-358, 2012
- [20] A. Yildiz, S. B. Lisesivdin, M. Kasap, D. Mardare, "Electrical properties of TiO<sub>2</sub> thin films", Journal of Non-Crystalline Solids, Vol. 354, No. 45-46, pp. 4944-4947, 2008
- [21] P. Chowdhury, H. C. Barshilia, N. Selvakumar, B. Deepthi, K. S. Rajam, A. R. Chaudhuri, S. B. Krupanidhi, "The structural and electrical properties of TiO<sub>2</sub> thin films prepared by thermal oxidation", Physica B: Condensed Matter, Vol. 403, No. 19-20, pp. 3718-3723, 2008
- [22] M. S. P. Sarah, M. Z. Musa, M. N. Asiah, M. Rusop, "Electrical conductivity characteristics of TiO<sub>2</sub> thin film", 2010 International Conference on Electronic Devices, Systems and Applications, Kuala Lumpur, Malaysia, April 11-14, 2010
- [23] K. Conder, Electronic and Ionic Conductivity in Metal Oxides, Laboratory for Developments and Methods, Paul Scherrer Institut, 2012
- [24] J. Marugan, R. Van Grieken, O. M. Alfano, A. E. Cassano, "Optical and physicochemical properties of silica-supported TiO<sub>2</sub> photocatalysts", AIChE Journal, Vol. 52, No. 8, pp. 2832-2843, 2006
- [25] J. Marugan, R. van Grieken, A. E. Cassano, O. M. Alfano, "Quantum efficiency of cyanide photooxidation with TiO<sub>2</sub>/SiO<sub>2</sub> catalysts: Multivariate analysis by experimental design", Catalysis Today, Vol. 129, No. 1-2, pp. 143-151, 2007
- [26] J. Marugan, R. Van Grieken, A. E. Cassano, O. M. Alfano, "Comparison of empirical and kinetic modeling of the photocatalytic oxidation of cyanide", International Journal of Chemical Reactor Engineering, Vol. 5, No. 1, 2007
- [27] M. R. Hoffmann, S. T. Martin, W. Choi, D. W. Bahnemann, "Environmental Applications of Semiconductor Photocatalysis", Chemical Reviews, Vol. 95, No. 1, pp. 69-96, 1995
- [28] V. Augugliaro, V. Loddo, G. Marci, L. Palmisano, M. J. Lopez-Munoz, "Photocatalytic oxidation of cyanides in aqueous titanium dioxide suspensions", Journal of Catalysis, Vol. 166, No. 2, pp. 272-283, 1997
- [29] K. Chiang, R. Amal, T. Tran, "Photocatalytic oxidation of cyanide: Kinetic and mechanistic studies", Journal of Molecular Catalysis A: Chemical, Vol. 193, No. 1-2, pp. 285-297, 2003
- [30] S. N. Frank, A. J. Bard, "Heterogeneous photocatalytic oxidation of cyanide ion in aqueous solutions at titanium dioxide powder", Journal of the American Chemical Society, Vol. 99, No. 1, pp. 303-304, 1977
- [31] J. Marugan, R. van Grieken, A. E. Cassano, O. M. Alfano, "Scaling-up of slurry reactors for the photocatalytic oxidation of cyanide with TiO<sub>2</sub> and silica-supported TiO<sub>2</sub> suspensions", Catalysis Today, Vol. 144, No. 1-2, pp. 87-93, 2009
- [32] A. Vidal, S. Malato, J. Blanco, "Procesos solares, fotocatalíticos en el tratamiento de efluentes", Ingeniería Química, Vol. 34, No. 386, pp. 106-111, 2002 (in Spanish)
- [33] J. Marugan, R. van Grieken, A. E. Cassano, O. M. Alfano, "Intrinsic kinetic modeling with explicit radiation absorption effects of the photocatalytic oxidation of cyanide with TiO<sub>2</sub> and silica-supported TiO<sub>2</sub> suspensions", Applied Catalysis B: Environmental, Vol. 85, No. 1-2, pp. 48-60, 2008
- [34] I. Salvado-Estivill, D. M. Hargreaves, G. Li Puma, "Evaluation of the Intrinsic Photocatalytic Oxidation Kinetics of Indoor Air Pollutants", Environmental Science & Technology, Vol. 41, No. 6, pp. 2028-2035, 2007
- [35] M. Rodriguez, S. Malato, C. Pulgarin, S. Contreras, D. Curco, J. Gimenez, S. Esplugas, "Optimizing the solar photo-Fenton process in the treatment of contaminated water. Determination of intrinsic kinetic constants for scale-up", Solar Energy, Vol. 79, No. 4, pp. 360-368, 2005
- [36] O. M. Alfano, M. I. Cabrera, A. E. Cassano, "Photocatalytic reactions involving hydroxyl radical attack. I. Reaction kinetics formulation with explicit photon absorption effects", Journal of Catalysis, Vol. 172, pp. 370-379, 1997
- [37] J. R. R. Gurr, A. S. S. Wang, C. H. H. Chen, K. Y. Y. Jan, "Ultrafine titanium dioxide particles in the absence of photoactivation can induce oxidative damage to human bronchial epithelial cells", Toxicology, Vol. 213, No. 1-2, pp. 66-73, 2005
- [38] R. L. Pozzo, M. A. Baltanas, A. E. Cassano, "Supported titanium oxide as photocatalyst in water decontamination: State of the art", Catalysis Today, Vol. 39, No. 3, pp. 219-231, 1997
- [39] M. L. Satuf, R. J. Brandi, A. E. Cassano, O. M. Alfano, "Scaling-up of slurry reactors for the photocatalytic degradation of 4-chlorophenol", Catalysis Today, Vol. 129, No. 1-2, pp. 110-117, 2007
- [40] X. Sun, Y. Charles Guan, K. N. Han, "Electrochemical behavior of the dissolution of gold-silver alloys in cyanide solutions", Metallurgical and Materials Transactions B, Vol. 27, No. 3, pp. 355-361, 1996
- [41] A. Gilat, V. Subramaniam, "Numerical methods for engineers and scientists: an introduction with applications using MATLAB", in: Numerical Methods for Engineers and Scientists: An Introduction with Applications Using MATLAB, Wiley Global Education, 2011
- [42] S. C. Chapra, R. P. Canale, Numerical methods for engineers, McGraw-Hill, 2015
- [43] T. Y. Wei, C. C. Wan, "Heterogeneous photocatalytic oxidation of phenol with titanium dioxide powders", Industrial & Engineering Chemistry Research, Vol. 30, No. 6, pp. 1293-1300, 1991
- [44] K. Okamoto, Y. Yamamoto, H. Tanaka, M. Tanaka, A. Itaya, "Heterogeneous Photocatalytic Decomposition of Phenol over TiO<sub>2</sub> Powder", Bulletin of the Chemical Society of Japan, Vol. 58, No. 7, pp. 2015-2022, 1985
- [45] F. Akbal, A. N. Onar, "Photocatalytic degradation of phenol", Environmental Monitoring and Assessment, Vol. 83, No. 3, pp. 295-302, 2003